Scanning probe nanoscale patterning of highly ordered pyrolytic graphite

2010 Nanotechnology 21 095306

(http://iopscience.iop.org/0957-4484/21/9/095306)

Nanotechnology **21** (2010) 095306 (4pp) doi:10.1088/0957-4484/21/9/095306

Scanning probe nanoscale patterning of highly ordered pyrolytic graphite

Norimasa Yoshimizu, Bryan Hicks, Amit Lal and Clifford R Pollock

SonicMEMS Laboratory, School of Electrical and Computer Engineering, Cornell University, Ithaca, NY 14853, USA

E-mail: ny22@cornell.edu

Received 13 November 2009, in final form 19 January 2010
Published 8 February 2010
Online at stacks.iop.org/Nano/21/095306

Abstract

In this work we present precision scanning probe etching of highly ordered pyrolytic graphite. We corroborate that the lithography is due to an electrochemical, polarity-dependent, meniscus-mediated etching of the carbon surface. By changing the etching temperature, we are able to reduce the feature size by 24%. External feedback control and probe tip cleaning enables desired cut patterns with high precision. Using a feedback-controlled atomic force microscope, we demonstrate an array of 105 trenches using 370 etching operations, with 136 ± 6 and 183 ± 5 nm precision over an area of 2.5 μm $\times$ 2.5 μm. This results in a precision of 4.4% and 2.7%, respectively.

(Some figures in this article are in colour only in the electronic version)

1. Introduction

The recent growth of interest in carbon-based devices [1] is in part motivated by the nanoscale control of electrical properties with size. For example, this size control in nanoribbons requires atomic ($\approx$1.4 Å) control of their dimensions [2]. Nanofabrication with scanning probe microscopes is an attractive method for high resolution nanofabrication beyond photo- or electron-lithographic methods, perhaps down to atom level engineering. There are a number of papers on scanning probe nanofabrication of HOPG, with a variety of empirical observations and proposed etching mechanisms [3–5]. In all cases, a scanning probe approaches the surface of the HOPG and a bias voltage is applied between the sample and the tip. Both carbon oxidation resulting in a convex protrusion and carbon etching resulting in a small concave pit are observed. These processes can be used as a method to fabricate nanoscale carbon-based devices. The origins of graphite etching could be defects induced by an argon plasma [6], atomic oxygen [7], or due to knock-on collisions from energetic electrons [8]. These processes may have secondary effects in scanning probe etching of graphite, but polarity, temperature, and electric current data suggest that an electrochemical reaction is the fundamental origin. Here, we report on the chemistry of scanning probe electrochemical etching of highly ordered pyrolytic graphite and the demonstration of numerous, precise nanofabrications.

2. Scanning probe etching of graphite

The process of scanning probe microscope graphite etching is due to an aqueous electrochemical oxidation and removal of surface carbon atoms. The water is supplied by the meniscus that forms between the carbon surface and the scanning probe tip from the ambient moisture. As a result, HOPG etching does not occur under vacuum. This is best described by the Pourbaix diagram for carbon, which shows a narrow region of stability at low potentials [9]. The main graphite etching reaction is the generation of carbon dioxide [10–12],

$$C + 2H_2O \rightleftharpoons 4H^+ + 4e^- + CO_2, \quad (1)$$

which is essentially an irreversible reaction whose rate is increased at positive carbon, or cathode, voltages. At high bias voltages, the carbon is etched rapidly. At low bias voltages the carbon can be oxidized rather than etched: while the Pourbaix diagram indicates the possibility of etching at low voltages, the chemical kinetics favor the oxidation reaction [13]. We have been able to etch graphene at voltages as small as +2 V sample bias. At the reverse polarities, the Pourbaix diagram shows the possibility of the generation of methane by combining carbon with four hydrogen ions and four free electrons, but this is a highly unlikely reaction. This results in HOPG cutting only at a positive sample bias, as seen in figure 1.

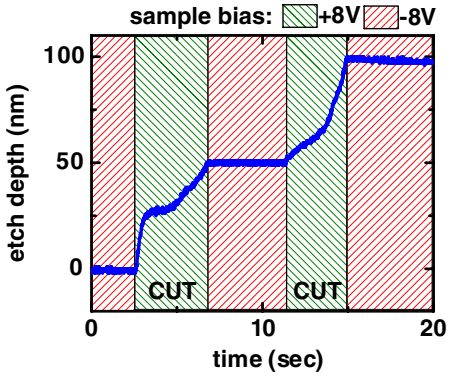

Figure 1. Etch depth as sample bias is switched between +8 and −8 V, demonstrating polarity dependence of the electrochemical etch. When the sample bias is +8 V with respect to the scanning probe tip, the essentially irreversible reaction in equation (1) etches the graphite: the tip etches into the HOPG. The opposite polarity, −8 V, results in no etching of the graphite as the generation of methane requires the carbon to react with four hydrogen ions and four free electrons: the tip position does not change. The polarity-dependent etching of HOPG allows for electrochemical cleaning of the probe and possibly graphite annealing.

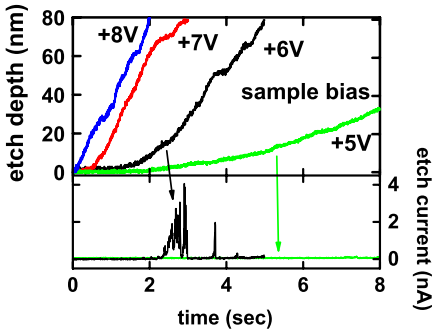

Figure 2. Etch profiles at several sample bias voltages. Note the constant etch rates, especially at +7 and +8 V sample bias, which imply a constant activity coefficient. The current is also measured as the tip etches the carbon. At a bias of +5 V, the hydrogen ion and free electron currents are not measured by the scanning probe tip. However at a bias of +6 V, the tip and substrate capture some of the current.

It is found that, generally, the hydrogen ions and free electrons in reaction (1) combine quickly during the etching process and disperse as hydrogen gas. First, note that electrochemical etching at the scanning probe involves etching carbon with a small volume of solvent as the meniscus. Given the amount of carbon that is typically etched and the resultant amount of ionic hydrogen, it would be possible for the molal ionic strength to range up to tens of thousands. Even for a much smaller range, the activity coefficient for reaction (1) would change by an order of magnitude (cf [14]). However, the etch profiles in figure 2 show that the etch rate is linear, indicating that the reaction rate and therefore the activity coefficient is constant. Second, it is possible to etch graphite without current, as seen in figure 2. Free charge is only seen at higher cutting voltages, where some of the hydrogen ions and the free charge can be pulled to the tip and substrate, respectively.

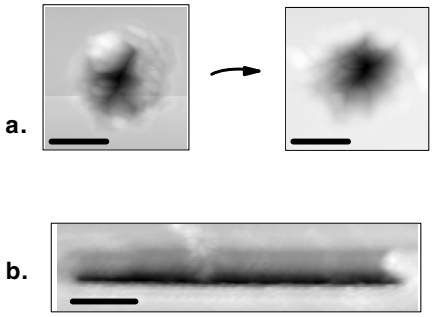

Figure 3. (a) Tapping mode image of a large hole (scale bars show 50 nm) showing some crevice structure. After imaging, three contact mode scans were made of the hole. The subsequent tapping mode image shows removal of water. (b) Tapping mode image of a smooth line (scale bar shows 100 nm).

Operating the atomic force microscope (AFM) in the tapping mode, in figure 3 we show fine structure of HOPG etching that has previously been unobserved. While contact mode images tend to show very smooth pits, the tapping mode images typically show crevice structure inside the pit. Figure 3(b) also shows a tapping mode image of a smooth line cut by moving the tip along the surface. In addition, by comparing tapping mode images to contact mode images we find that water is present after features are cut into the HOPG. This is confirmed as the water can be removed by running the tip across the water under contact or by pumping down the chamber to vacuum then reimaging the HOPG; see figure 3(a). The presence of the water is surprising, as HOPG is hydrophobic. This may be a combined effect from surface modifications to the carbon and a change in pH of the water due to the etching process. The etching process in addition to removing carbon can also oxidize the carbon, which will decrease its hydrophobicity [15]. Graphite's wettability can also be raised by increasing the acidity [16] caused by the formation of carbonic acid and carbonates,

$$C + 3H_2O \rightleftharpoons H_2CO_3 \tag{2}$$

$$C + 3H_2O \rightleftharpoons HCO_3^- + H^+ \tag{3}$$

$$C + 3H_2O \rightleftharpoons CO_3^{--} + 2H^+, \tag{4}$$

as evident in the Pourbaix diagram for carbon.

While we expect the reaction in equation (1) to cleanly etch the carbon without residuals, energy dispersive x-ray spectroscopy with an electron beam microprobe shows the presence of carbon on the AFM tip surface. After several hundred hole etches, the deposited carbon is clearly visible in an SEM image of the tip. The increased tip diameter results in poor imaging and lithographic resolution. We found that this can be simply remedied by applying a large negative sample bias, opposite in polarity from the voltages used in HOPG etching. As demonstrated above, large reverse biases can be applied without etching the HOPG. This process was used by Spinney *et al* [17] as a method of carbon deposition onto a gold surface. We find, however, that AFM images of the HOPG surface before and after cleaning the tip are identical. We intermittently clean the AFM probe in this manner to maintain

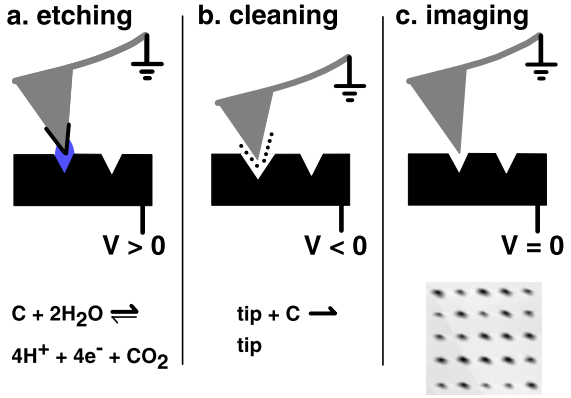

Figure 4. Schematic summary of modes of operation for AFM graphite nanolithography: (a) etching occurs at positive sample bias voltages with a meniscus formed between the tip and the sample via an electrochemical etch chemistry. While etching, carbon deposits form on the AFM tip. (b) Tip cleaning of carbon deposits occurs at negative sample bias voltages. (c) Image scans are at zero bias voltages.

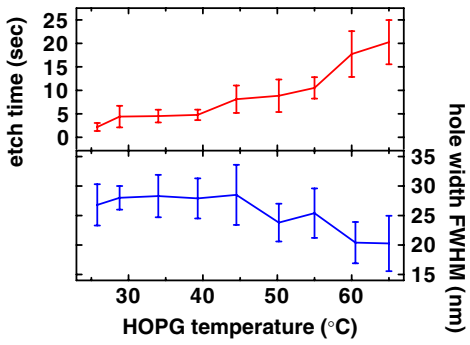

Figure 5. Temperature dependence of HOPG etching with $V_H = 10.5$ V, $V_L = 9$ V. Top shows a decrease in cutting rate as the temperature of the HOPG is raised. A decrease in cutting rate can be offset by increasing the sample voltage. Bottom shows improved lithography resolution as the temperature of HOPG is raised. Increased temperature leads to increased volatility due to evaporation at the edges of the meniscus, resulting in a smaller meniscus resulting in a smaller etch feature size but also much slower etch rates.

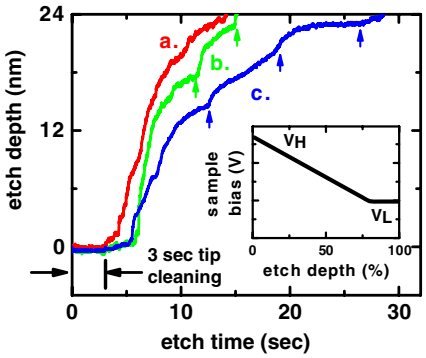

Figure 6. Etch profiles using etch control depicted in inset with $V_H = +11.5$ V and $V_L = +11$ V; a three second tip cleaning at -10 V sample bias precedes all the etches. (a) An optimal etching profile, where the etching depth and deceleration are smooth. (b) The etch begins very slowly for 2.8 s. Arrows indicate pauses during etching, possibly due to disappearance and reappearance of the meniscus. (c) Very slow etch with several etching pauses. Even with the same parameters as (a) and (b), the etch time is twice that of the nominal etch in (a). Inset shows control feedback for precision etching of graphite. The applied bias starts at a large V_H, rapidly initiating the cut and etching most of the desired depth. The applied bias decreases linearly with etching depth, until at some percentage of the desired etch depth the applied bias is set to a low V_L, typically a volt below V_H. The V_L yields a well-controlled etch depth and width by slowing down the etch rate.

a clean, sharp tip over several hundred writes. Additionally the negative sample bias allows non-destructive current injection from the tip into the graphite, which will anneal the graphite edges by Joule heating [18]. We summarize the etching, cleaning, and scanning modes of operation in figure 4.

The lithographic feature size is determined by the size of the meniscus that forms between the scanning probe tip and the HOPG surface. The meniscus size is mainly determined by the environment, probe parameters, and tip height [19]. The temperature dependence can be exploited to control the feature size. As the temperature of the HOPG surface increases, the evaporation rate at the edges of the meniscus increases, resulting in a narrower meniscus and smaller feature size. The data are shown in figure 5, where a 35 °C increase in HOPG temperature results in a 24% decrease in the full width half maximum of 24 nm deep holes. The Arrhenius equation predicts an increase in the etching rate as the surface temperature is elevated. Instead, the etching rate slows at higher temperature due to increased instability of the meniscus. The thermally reduced meniscus yields smaller feature sizes but increased etch times. We estimate that the average etch rate decreases from a maximum 2×10^6 atoms s^{-1} to a minimum 2×10^5 atoms s^{-1}.

3. Precision writing of a line array

Scanning probe etching of HOPG is driven by the tip–substrate meniscus, and as a result is sensitive to the tip shape and surface, tip–sample separation, environment, applied bias, etch time, and temperature. Slight variations among tips might require the applied bias to vary from 6 up to 15 V or more before a given tip will etch HOPG. Even the same tip will etch inconsistently over time due to changes in a variety of these parameters. In order to nanofabricate many features consistently, it is necessary to incorporate a feedback control system. We implemented a digital control system that monitored the AFM piezo-height position and controlled the applied bias voltage. We used conductive AFM tips with a platinum thin film: platinum has been found to catalyze the electrochemical corrosion of carbon [20, 21]. The control is shown in the inset of figure 6, where a voltage bias is applied to the substrate based on the cut depth. The cutting begins at a larger voltage V_H, typically more than +10 V. Higher biases consistently initiate the carbon etching and etch at a more rapid rate. However, fast etches lasting less than a second result in inconsistent dimensions and more tip damage, possibly due to more mechanical damage and deposited carbon. Therefore, the bias voltage is decreased to a smaller voltage V_L, typically one or two volts smaller than V_H, when the tip has reached 80–90%

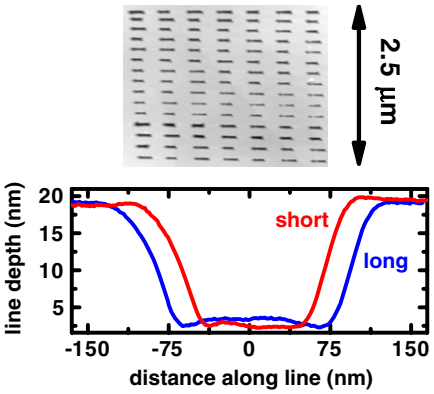

Figure 7. AFM image shows large array of 18.3 ± 3 nm deep etched lines in HOPG. Lines are randomly selected to be 136 and 183 nm in length, yielding 6 nm (4.4%) and 5 nm (2.7%) precision, respectively. Figure below shows sample cross sections of short and long lines.

of the total desired etch depth. Etching at V_L results in slower, smoother cuts with well-controlled etch dimensions. Etching at too small of a voltage impractically increases fabrication times, and the increased time allows longer lateral drifts in the tip position resulting in degraded feature quality. In addition, the graphite may undergo oxidation rather than etching, as described above.

Using this feedback control loop, several examples of etches are shown in figure 6. Etches (a)–(c) all start with a three second tip cleaning by applying a −10 V sample bias voltage. Etch (a) is an optimal etching profile. The etch starts immediately after the tip cleaning, and etches quickly before slowing down just before the desired etch height is reached. Etch (b) shows some variation from an optimal etch profile. The etching begins very slowly (7 Å s^{-1}) for 2.8 s until the etch rate suddenly increases to a substantial rate. The etch also shows two pauses, indicated by arrows. An etch will sometimes slow or even stop for several seconds, then suddenly resume etching into the carbon surface. This slow decrease and abrupt jump in etching rate may be a result of the loss and reformation of the tip–sample meniscus. Etch (c) shows a large deviation from the etch profiles of (a) and (b). The initial delay is slightly less than that of (b), but the overall etch rate is lower. Etching ceases several times, once as long as five seconds, and in the end its total etch time is twice as long as that for (a).

We fabricated an array of trenches to demonstrate the scalability of our precision HOPG-patterning technique. These lines were cut by measuring the HOPG height at the endpoints and linearly interpolating a desired cut depth along the line. The lines are three or four pixel widths, where a pixel is about 40 nm wide. The line length was chosen at random by the computer immediately before each one was fabricated. The values for V_H and V_L were +11.5 and +11 V, but offsets were added to these voltages during fabrication to keep the etch time for each line at around 40 s. A −10 V sample bias was applied for 3 s to clean the tip before etching each line.

In order to assess the precision of the fabricated lines, we measured the depth and full width at half maximum depths using AFM scans. The result from a seven by fifteen array of lines is 136 ± 6 and 183 ± 5 nm, with etch depths that are 18.3 ± 3 nm. Figure 7 shows typical profiles of a long and a short line sampled from this array. There is a consistent asymmetry in the edge slopes due to an imaging artifact.

4. Conclusion

We have demonstrated feedback-controlled nanofabrication of a 105 line array in HOPG, using some 370 etching operations on an atomic force microscope. The lines were randomly selected to be of two lengths which were precise to within 4.4% and 2.7%, or 6 nm and 5 nm, respectively; the depths were measured to be 18.3 ± 3 nm. The precision of nanofabrication was maintained by a bias voltage etch depth feedback control loop of the etching rate. In addition, etching results in carbon build-up on the tip which reduces fabrication and imaging precision. A negative sample bias was applied to remove carbon residuals from the tip without sample damage. This work demonstrates that non-prototypical scanning probe nanofabrication for carbon-based devices is possible.

Acknowledgments

This work was generously funded by DARPA/MTO's TBN program.

References

[1] Geim A K and Novoselov K S 2007 *Nat. Mater.* **6** 183–91
[2] Son Y-W, Cohen M L and Louie S G 2006 *Phys. Rev. Lett.* **97** 216803
[3] Albrecht T R, Dovek M M, Kirk M D, Lang C A, Quate C F and Smith D P E 1989 *Appl. Phys. Lett.* **55** 1727–9
[4] Park J G, Zhang C, Liang R and Wang B 2007 *Nanotechnology* **18** 405306
[5] Jiang Y and Guo W 2008 *Nanotechnology* **19** 345302
[6] Rousseau B, Estrade-Szwarckopf H, Thomann A-L and Brault P 2003 *Appl. Phys.* A **77** 591–7
[7] Nicholson K T, Minton T K and Sibener S J 2005 *J. Phys. Chem.* B **109** 8476–80
[8] Banhart F 1999 *Rep. Prog. Phys.* **62** 1181–21
[9] Pourbaix M 1974 *Atlas of Electrochemical Equilibria in Aqueous Solutions* 2nd edn (New York: National Association of Corrosion Engineers) pp 449–57
[10] Mizutani W, Inukai J and Ono M 1990 *Japan. J. Appl. Phys.* **29** L815–7
[11] McCarley R L, Hendricks S A and Bard A J 1992 *J. Phys. Chem.* **96** 10089–92
[12] Matsumoto M, Manako T and Imai H 2009 *J. Electrochem. Soc.* **156** B1208–11
[13] Kozlowski C and Sherwood P M A 1984 *J. Chem. Soc., Faraday Trans.* 1 **80** 2099–107
[14] Pitzer K S 1991 *Activity Coefficients in Electrolyte Solutions* (Boca Raton, FL: CRC Press) pp 75–278
[15] Ebbesen T W 1995 *J. Phys. Chem. Solids* **57** 951–5
[16] Gribanova E V, Zhukov A N, Antonyuk I E, Benndorf C and Baskova E N 2000 *Diamond Relat. Mater.* **9** 1–6
[17] Spinney P S, Collins S D and Smith R L 2007 *Nano Lett.* **7** 1512–5
[18] Jia X *et al* 2009 *Science* **323** 1701–5
[19] Jang J, Schatz G C and Ratner M A 2002 *Phys. Rev. Lett.* **92** 085504
[20] Willsau J and Heitbaum J 1984 *J. Electroanal. Chem.* **161** 93–101
[21] Roen L M, Paik C H and Jarvi T D 2004 *Electrochem. Solid-State Lett.* **17** A19–22